

Energy-Based Continuous Inverse Optimal Control

Yifei Xu, Jianwen Xie, Tianyang Zhao, Chris Baker, Yibiao Zhao and Ying Nian Wu

Abstract—The problem of continuous optimal control (over finite time horizon) is to minimize a given cost function over the sequence of continuous control variables. The problem of continuous inverse optimal control is to learn the unknown cost function from expert demonstrations. In this article, we study this fundamental problem in the framework of energy-based model, where the observed expert trajectories are assumed to be random samples from a probability density function defined as the exponential of the negative cost function up to a normalizing constant. The parameters of the cost function are learned by maximum likelihood via an “analysis by synthesis” scheme, which iterates the following two steps: (1) Synthesis step: sample the synthesized trajectories from the current probability density using the Langevin dynamics via back-propagation through time. (2) Analysis step: update the model parameters based on the statistical difference between the synthesized trajectories and the observed trajectories. Given the fact that an efficient optimization algorithm is usually available for an optimal control problem, we also consider a convenient approximation of the above learning method, where we replace the sampling in the synthesis step by optimization. To make the sampling or optimization more efficient, we propose to train the energy-based model simultaneously with a top-down trajectory generator via cooperative learning, where the trajectory generator is used to fast initialize the sampling step or optimization step of the energy-based model. We demonstrate the proposed methods on autonomous driving tasks, and show that it can learn suitable cost functions for optimal control.

Index Terms—Inverse Optimal Control; Energy-based models; Langevin dynamics; Cooperative learning.



1 INTRODUCTION

1.1 Background and motivation

THE problem of continuous optimal control has been extensively studied. In this paper, we study the control problem of finite time horizon, where the trajectory is over a finite period of time. In particular, we focus on the problem of autonomous driving as a concrete example. In continuous optimal control, the control variables or actions are continuous. The dynamics is known. The cost function is defined on the trajectory and is usually in the form of the sum of stepwise costs and the cost of the final state. We call such a cost function Markovian. The continuous optimal control seeks to minimize the cost function over the sequence of continuous control variables or actions, and many efficient algorithms have been developed for various optimal control problems [1]. For instance, in autonomous driving, the iLQR (iterative linear quadratic regulator) algorithm is a commonly used optimization algorithm [2], [3]. We call such an algorithm the built-in optimization algorithm for the corresponding control problem.

In applications such as autonomous driving, the dynamics is well defined by the underlying physics and mechanics. However, it is a much harder problem to design or specify the cost function. One solution to this problem is to learn the cost function from

expert demonstrations by observing their sequences of actions. Learning the cost function in this way is called continuous inverse optimal control problem.

In this article, we study the fundamental problem of continuous inverse optimal control in the framework of energy-based model. Originated from statistical physics, an energy-based model is a probability distribution where the probability density function is in the form of exponential of the negative energy function up to a normalizing constant. Instances with low energies are assumed to be more likely according to the model. For continuous inverse optimal control, the cost function plays the role of energy function, and the observed expert sequences are assumed to be random samples from the energy-based model so that sequences with low costs are more likely to be observed. We can choose the cost function either as a linear combination of a set of hand-designed features, or a non-linear and non-markovian neural network. The goal is to learn the parameters of the cost function from the expert sequences.

The parameters can be learned by the maximum likelihood method in the context of the energy-based model. The maximum likelihood learning algorithm follows an “analysis by synthesis” scheme, which iterates the following two steps: (1) Synthesis step: sample the synthesized trajectories from the current probability distribution using the Langevin dynamics [4]. The gradient computation in the Langevin dynamics can be conveniently and efficiently carried out by back-propagation through time. (2) Analysis step: update the model parameters based on the statistical difference between the synthesized trajectories and the observed trajectories. Such a learning algorithm is very general, and it can learn complex cost functions such as those defined by the neural networks.

For an optimal control problem where the cost function is of the Markovian form, a built-in optimization algorithm is usually already available, such as the iLQR algorithm for autonomous

- *Y. Xu is with the Department of Statistics, University of California, Los Angeles, CA 90095, USA. E-mail: fei960922@ucla.edu*
- *J. Xie is with the Cognitive Computing Lab, Baidu Research, Bellevue, WA 98004, USA. E-mail: jianwen@ucla.edu*
- *T. Zhao is with the Department of Statistics, University of California, Los Angeles, CA 90095, USA. E-mail: tyzhao@ucla.edu*
- *C. Baker is with iSee Inc., Cambridge, MA 02139, USA. E-mail: chris-baker@isee.ai*
- *Y. Zhao is with iSee Inc., Cambridge, MA 02139, USA. E-mail: yz@isee.ai*
- *Y. N. Wu is with the Department of Statistics, University of California, Los Angeles, CA 90095, USA. E-mail: ywu@stat.ucla.edu*

driving. In this case, we also consider a convenient modification of the above learning method, where we change the synthesis step (1) into an optimization step while keeping the analysis step (2) unchanged. We give justifications for this optimization-based method, although we want to emphasize that the sampling-based method is still more fundamental and principled, and we treat optimization-based method as a convenient modification.

We also train the energy-based model with a trajectory generator as a fast initializer for the Langevin sampling of the energy-based model in a cooperative learning scheme.

We demonstrate the proposed energy-based continuous optimal control methods on autonomous driving and show that the proposed methods can learn suitable cost functions for optimal control.

1.2 Related work

The following are research themes related to our work.

(1) Maximum entropy framework. Our work follows the maximum entropy framework of [5] for learning the cost function. Such a framework has also been used previously for generative modeling of images [6] and Markov logic network [7]. In this framework, the energy function is a linear combination of hand-designed features. Recently, [8] generalized this framework to deep version. In these methods, the state spaces are discrete, where dynamic programming schemes can be employed to calculate the normalizing constant of the energy-based model. In our work, the state space is continuous, where we use Langevin dynamics via back-propagation through time to sample trajectories from the learned model. We also propose an optimization-based method where we use gradient descent or a built-in optimal control algorithm as the inner loop for learning.

(2) ConvNet energy-based models (EBM). Recently, [9], [10], [11] applied energy-based model to various generative modeling tasks, where the energy functions are parameterized by ConvNets [12], [13]. Our method is different from ConvNet EBM. The control variables in our method form a time sequence. In gradient computation for Langevin sampling, back-propagation through time is used. Also, we propose an optimization-based modification and give justifications.

(3) Inverse reinforcement learning. Most of the inverse reinforcement learning methods [14], [15], including adversarial learning methods [15], [16], [17], [18], involve learning a policy in addition to the cost function. In our work, we do not learn any policy. We only learn a cost function, where the trajectories are sampled by the Langevin dynamics or obtained by gradient descent or a built-in optimal control algorithm.

(4) Continuous inverse optimal control (CIOC). The CIOC problem has been studied by [19] and [20]. In [19], the dynamics is linear and the cost function is quadratic, so that the normalizing constant can be computed by a dynamic programming scheme. In [20], the Laplace approximation is used for approximation. However, the accuracy of the Laplace approximation is questionable for complex cost function. In our work, we assume general dynamics and cost function, and we use Langevin sampling for maximum likelihood learning without resorting to Laplace approximation.

(5) Trajectory prediction. A recent body of research has been devoted to supervised learning for trajectory prediction [21], [22], [23], [24], [25], [26]. These methods directly predict the coordinates and they do not consider control and dynamic models. As a result, they cannot be used for inverse optimal control.

1.3 Contributions

The contributions of our work are as follows. (1) We propose an energy-based method for continuous inverse optimal control based on Langevin sampling via back-propagation through time. (2) We also propose an optimization-based method as a convenient approximation. (3) We evaluate the proposed methods on autonomous driving tasks for both single-agent system and multi-agent system, with both linear cost function and neural network non-linear cost function. (4) We also propose to train an energy-based model together with a trajectory generator, which serves as a fast initializer for Langevin sampling, in a cooperative learning scheme.

2 ENERGY-BASED INVERSE OPTIMAL CONTROL

2.1 Optimal control

We study the finite horizon control problem for discrete time $t \in \{1, \dots, T\}$. Let x_t be the state at time t . Let $\mathbf{x} = (x_t, t = 1, \dots, T)$. Let u_t be the continuous control variable or action at time t . Let $\mathbf{u} = (u_t, t = 1, \dots, T)$. The dynamics is assumed to be deterministic, $x_t = f(x_{t-1}, u_t)$, where f is given, so that \mathbf{u} determines \mathbf{x} . The trajectory is $(\mathbf{x}, \mathbf{u}) = (x_t, u_t, t = 1, \dots, T)$. Let e be the environment condition. We assume that the recent history $h = (x_t, u_t, t = -k, \dots, 0)$ is known.

The cost function is $C_\theta(\mathbf{x}, \mathbf{u}, e, h)$ where θ consists of the parameters that define the cost function. Its special case is of the linear form $C_\theta(\mathbf{x}, \mathbf{u}, e, h) = \langle \theta, \phi(\mathbf{x}, \mathbf{u}, e, h) \rangle$, where ϕ is a vector of hand-designed features, and θ is a vector of weights for these features. We can also parametrize C_θ by a neural network. The problem of optimal control is to find \mathbf{u} to minimize $C_\theta(\mathbf{x}, \mathbf{u}, e, h)$ with given e and h under the known dynamics f . The problem of inverse optimal control is to learn θ from expert demonstrations $D = \{(\mathbf{x}_i, \mathbf{u}_i, e_i, h_i), i = 1, \dots, n\}$.

2.2 Energy-based probabilistic model

The energy-based model assumes the following conditional probability density function

$$p_\theta(\mathbf{u}|e, h) = \frac{1}{Z_\theta(e, h)} \exp[-C_\theta(\mathbf{x}, \mathbf{u}, e, h)], \quad (1)$$

where $Z_\theta(e, h) = \int \exp[-C_\theta(\mathbf{x}, \mathbf{u}, e, h)] d\mathbf{u}$ is the normalizing constant. Recall that \mathbf{x} is determined by \mathbf{u} according to the deterministic dynamics, so that we only need to define probability density on \mathbf{u} . The cost function C_θ serves as the energy function. For expert demonstrations D , \mathbf{u}_i are assumed to be random samples from $p_\theta(\mathbf{u}|e_i, h_i)$, so that \mathbf{u}_i tends to have low cost $C_\theta(\mathbf{x}, \mathbf{u}, e_i, h_i)$.

2.3 Sampling-based inverse optimal control

We can learn the parameters θ by maximum likelihood. The log-likelihood is

$$L(\theta) = \frac{1}{n} \sum_{i=1}^n \log p_\theta(\mathbf{u}_i|e_i, h_i). \quad (2)$$

We can maximize $L(\theta)$ by gradient ascent, and the learning gradient is

$$L'(\theta) = \frac{1}{n} \sum_{i=1}^n \left[\mathbb{E}_{p_\theta(\mathbf{u}|e_i, h_i)} \left(\frac{\partial}{\partial \theta} C_\theta(\mathbf{x}, \mathbf{u}, e_i, h_i) \right) - \frac{\partial}{\partial \theta} C_\theta(\mathbf{x}_i, \mathbf{u}_i, e_i, h_i) \right], \quad (3)$$

which follows from the fact that $\frac{\partial}{\partial \theta} \log Z_\theta(e, h) = -\mathbb{E}_{p_\theta(\mathbf{u}|e, h)} \left(\frac{\partial}{\partial \theta} C_\theta(\mathbf{x}, \mathbf{u}, e_i, h_i) \right)$.

In order to approximate the above expectation, we can generate multiple random sample $\tilde{\mathbf{u}}_i \sim p_\theta(\mathbf{u}|e, h)$, which generates the sampled trajectory $(\tilde{\mathbf{x}}_i, \tilde{\mathbf{u}}_i)$ by unfolding the dynamics. We estimate $L'(\theta)$ by

$$\hat{L}'(\theta) = \frac{1}{n} \sum_{i=1}^n \left[\frac{\partial}{\partial \theta} C_\theta(\tilde{\mathbf{x}}_i, \tilde{\mathbf{u}}_i, e_i, h_i) - \frac{\partial}{\partial \theta} C_\theta(\mathbf{x}_i, \mathbf{u}_i, e_i, h_i) \right], \quad (4)$$

which is the stochastic unbiased estimator of $L'(\theta)$. Then we can run the gradient ascent algorithm $\theta_{\tau+1} = \theta_\tau + \gamma_\tau \hat{L}'(\theta_\tau)$ to obtain the maximum likelihood estimate of θ , where τ indexes the time step, γ_τ is the step size. According to the Robbins-Monroe theory of stochastic approximation [27], if $\sum_\tau \gamma_\tau = \infty$ and $\sum_\tau \gamma_\tau^2 < \infty$, the algorithm will converge to a solution of $L'(\theta) = 0$. For each i , we can also generate multiple copies of $(\tilde{\mathbf{x}}_i, \tilde{\mathbf{u}}_i)$ from $p_\theta(\mathbf{u}|e_i, h_i)$ and average them to approximate the expectation in (3). A small number is sufficient because the averaging effect takes place over time.

In linear case, where $C_\theta(\mathbf{x}, \mathbf{u}, e, h) = \langle \theta, \phi(\mathbf{x}, \mathbf{u}, e, h) \rangle$, we have $\frac{\partial}{\partial \theta} C_\theta(\mathbf{x}, \mathbf{u}, e_i, h_i) = \phi(\mathbf{x}, \mathbf{u}, e, h)$, making $\hat{L}'(\theta) = \frac{1}{n} \sum_{i=1}^n [\phi(\tilde{\mathbf{x}}_i, \tilde{\mathbf{u}}_i, e_i, h_i) - \phi(\mathbf{x}_i, \mathbf{u}_i, e_i, h_i)]$. It is the statistical difference between the observed trajectories and synthesized trajectories. At maximum likelihood estimate, the two match each other.

The synthesis step that samples from $p_\theta(\mathbf{u}|e, h)$ can be accomplished by Langevin dynamics, which iterates the following steps:

$$\mathbf{u}_{s+1} = \mathbf{u}_s - \frac{\delta^2}{2} C'_\theta(\mathbf{x}_s, \mathbf{u}_s, e, h) + \delta \mathbf{z}_s, \quad (5)$$

where s indexes the time step, $C'_\theta(\mathbf{x}, \mathbf{u}, e, h)$ is the derivative with respect to \mathbf{u} . δ is the step size, and $\mathbf{z}_s \sim \mathcal{N}(0, I)$ independently over s , where I is the identity matrix of the same dimension as \mathbf{u} . The Langevin dynamics is an inner loop of the learning algorithm.

The gradient term $C'_\theta(\mathbf{x}, \mathbf{u}, e, h) = \partial C_\theta(\mathbf{x}, \mathbf{u}, e, h) / \partial \mathbf{u}$ is computed via back-propagation through time, where \mathbf{x} can be obtained from \mathbf{u} by unrolling the deterministic dynamics. The computation can be efficiently and conveniently carried out by auto-differentiation on the current deep learning platforms.

Notice that the state changes as the control is changed; at the same time, the change of control in the previous frame affects each cost later. Thus the derivative is calculated by back-propagation through time,

$$\frac{\partial}{\partial u_i} C_\theta = \sum_{i=t}^T \frac{\partial C_i}{\partial u_t} = \sum_{i=t}^T \frac{\partial C_i}{\partial x_i} \frac{\partial x_t}{\partial u_t} \prod_{j=t}^{i-1} \frac{\partial x_{j+1}}{\partial x_j} + \frac{\partial C_t}{\partial u_t}.$$

In practice, it can be computed conveniently and efficiently by auto-gradient frameworks.

2.4 Optimization-based inverse optimal control

We can remove the noise term in Langevin dynamics (5), to make it a gradient descent process, $\mathbf{u}_{s+1} = \mathbf{u}_s - \eta C'_\theta(\mathbf{x}_s, \mathbf{u}_s, e, h)$, and we can still learn the cost function that enables optimal control. This amounts to modifying the synthesis step into an optimization step. Moreover, a built-in optimization algorithm is usually already available for minimizing the cost function $C_\theta(\mathbf{x}, \mathbf{u}, e, h)$ over \mathbf{u} . For instance, in autonomous driving, a commonly used algorithm

is iLQR. In this case, we can replace the synthesis step by an optimization step, where, instead of sampling $\tilde{\mathbf{u}}_i \sim p_{\theta_i}(\mathbf{u}|e_i, h_i)$, we optimize

$$\tilde{\mathbf{u}}_i = \arg \min_{\mathbf{u}} C_\theta(\mathbf{x}, \mathbf{u}, e_i, h_i). \quad (6)$$

The analysis step remains unchanged. In this paper, we emphasize the sampling-based method, which is more principled maximum likelihood learning, and we treat the optimization-based method as a convenient modification. We will evaluate both learning methods in our experiments.

A justification for the optimization-based algorithms in the context of the energy-based model (1) is to consider its tempered version: $p_\theta(\mathbf{u}|e, h) \propto \exp[-C_\theta(\mathbf{x}, \mathbf{u}, e, h)/T]$, where T is the temperature. Then the optimized $\tilde{\mathbf{u}}$ that minimizes $C_\theta(\mathbf{x}, \mathbf{u}, e, h)$ can be considered the zero-temperature sample, which is used to approximate the expectation in (3).

Moment matching. For simplicity, consider the linear cost function $C_\theta(\mathbf{x}, \mathbf{u}, e, h) = \langle \theta, \phi(\mathbf{x}, \mathbf{u}, e, h) \rangle$. At the convergence of the optimization-based learning algorithm, which has the same analysis step (2) as the sampling-based algorithm, we have $\hat{L}'(\theta) = 0$, so that

$$\frac{1}{n} \sum_{i=1}^n \phi(\tilde{\mathbf{x}}_i, \tilde{\mathbf{u}}_i, e_i, h_i) = \frac{1}{n} \sum_{i=1}^n \phi(\mathbf{x}_i, \mathbf{u}_i, e_i, h_i), \quad (7)$$

where the left-hand side is the average of the optimal behaviors obtained by (6), and the right-hand side is the average of the observed behaviors. We want the optimal behaviors to match the observed behaviors on average. We can see the above point most clearly in the extreme case where all $e_i = e$ and all $h_i = h$, so that $\phi(\tilde{\mathbf{x}}, \tilde{\mathbf{u}}, e, h) = \frac{1}{n} \sum_{i=1}^n \phi(\mathbf{x}_i, \mathbf{u}_i, e, h)$, i.e., we want the optimal behavior under the learned cost function to match the average observed behaviors as far as the features of the cost function are concerned. Note that the matching is not in terms of raw trajectories but in terms of the features of the cost function. In this matching, we do not care about modeling the variabilities in the observed behaviors. In the case of different (e_i, h_i) for $i = 1, \dots, n$, the matching may not be exact for each combination of (e, h) . However, such mismatches may be detected by new features which can be included in the features of the cost function.

Adversarial learning. We can also justify this optimization-based algorithm outside the context of probabilistic model as adversarial learning. To this end, we re-think about the inverse optimal control, whose goal is not to find a probabilistic model for the expert trajectories. Instead, the goal is to find a suitable cost function for optimal control, where we care about the optimal behavior, not the variabilities of the observed behaviors. Define the value function

$$V = \frac{1}{n} \sum_{i=1}^n [C_\theta(\tilde{\mathbf{x}}_i, \tilde{\mathbf{u}}_i, e_i, h_i) - C_\theta(\mathbf{x}_i, \mathbf{u}_i, e_i, h_i)], \quad (8)$$

Then $\hat{L}'(\theta) = \frac{\partial}{\partial \theta} V$, so that the analysis step (2) increases V . Thus the optimization step and the analysis step play an adversarial game $\max_\theta \min_{\tilde{\mathbf{u}}_i, \forall i} V$, where the optimization step seeks to minimize V by reducing the costs, while the analysis step seeks to increase V by modifying the cost function. More specifically, the optimization step finds the minima of the cost functions to decrease V , whereas the analysis step shifts the minima toward the observed trajectories in order to increase V .

Algorithm 1 Energy-based IOC

- 1: **input** expert demonstrations $D = \{(\mathbf{x}_i, \mathbf{u}_i, e_i, h_i), \forall i\}$.
 - 2: **output** cost function parameters θ , and synthesized or optimized trajectories $\{(\tilde{\mathbf{x}}_i, \tilde{\mathbf{u}}_i), \forall i\}$.
 - 3: Let $\tau \leftarrow 0$, initialize θ .
 - 4: **repeat**
 - 5: **Synthesis step or optimization step:** synthesizing $\tilde{\mathbf{u}}_i \sim p_{\theta_t}(\mathbf{u}|e_i, h_i)$ by Langevin sampling, or optimizing $\tilde{\mathbf{u}}_i = \arg \min_{\mathbf{u}} C_{\theta}(\mathbf{x}, \mathbf{u}, e_i, h_i)$, by gradient descent (GD) or iLQR, and then obtain $\tilde{\mathbf{x}}_i$, for each i .
 - 6: **Analysis step:** update $\theta_{\tau+1} = \theta_{\tau} + \gamma_{\tau} \hat{L}'(\theta_{\tau})$, where \hat{L} is computed according to (4).
 - 7: $\tau \leftarrow \tau + 1$.
 - 8: **until** $\tau = \tau_{\max}$, the number of iterations.
-

2.5 Energy-based IOC algorithm

Algorithm 1 presents the learning algorithm.

We treat the sampling-based method as a more fundamental and principled method, and the optimization-based method as a convenient modification. In our experiments, we shall evaluate both sampling-based method using Langevin dynamics and optimization-based method with gradient descent (GD) or iLQR as optimizer.

3 JOINT TRAINING

3.1 A trajectory generator model as a fast initializer

Both sampling-based method via Langevin dynamics and optimization-based method via gradient descent are based on iterative process, which will benefit from good initialization. A good initial point can not only greatly shorten the number of iterative steps but also help find the optimal modes of the cost function. Therefore, we propose to train an energy-based model simultaneously with a trajectory generator model that serves as a fast initializer for the Langevin dynamics or gradient descent of the energy-based model.

The basic idea is to use the trajectory generator model to generate trajectories via ancestral sampling to initialize a finite step Langevin dynamics or gradient descent for training the energy-based model. In return, the trajectory generator model learns from how the Langevin dynamics or gradient descent updates the initial trajectories it generates. Such a cooperative learning strategy is proposed in [28], [29] for image generation.

To be specific, we propose the trajectory generator model that consists of the following two components

$$u_t = F_{\alpha}(x_{t-1}, \xi_t, e) \quad (9)$$

$$x_t = f(x_{t-1}, u_t) \quad (10)$$

where $t = 1, \dots, T$, (9) is the policy model, and (10) is the known dynamic function. $\xi_t \sim N(0, I)$ is the Gaussian noise vector. The Gaussian noise vectors at different times ($\xi_t, t = 1, \dots, T$) are independent of each other. Given the state x_t at time t along with the environment condition e , the policy model output the action u_{t+1} at time $t + 1$, where the noise vector ξ_t accounts for the randomness in the mapping from x_t to u_{t+1} . F_{α} is a multi-layer perceptron, where α is the model parameters of the network. The initial state x_0 is assumed to be given.

We denote $\boldsymbol{\xi} = (\xi_t, t = 1, \dots, T)$ and $p(\boldsymbol{\xi}) = \prod_{t=1}^T p(\xi_t)$. Given the state x_{t-1} and the environment condition e , although x_t is dependent on the action u_t , u_t is generated from ξ_t . In

fact, we can write the trajectory generator in a compact form, i.e., $\mathbf{u} = G_{\alpha}(\boldsymbol{\xi}, e, h)$, where G_{α} composes F_{α} and f over time, and we use $h = x_0$ for simplicity in our implementation.

The algorithm for joint training of the energy-based model and the trajectory generator is that: at each iteration, (1) we first sample $\boldsymbol{\xi}_i$ from the Gaussian prior distribution, and then generate the initial trajectories by $\hat{\mathbf{u}}_i = G_{\alpha}(\boldsymbol{\xi}_i, e_i, h_i)$ for $i = 1, \dots, n$. (2) Starting from the initial trajectories $\{\hat{\mathbf{u}}_i\}$, we sample from the energy-based model by running a finite number of Langevin steps or optimize the cost function by running a finite steps of gradient descent to obtain the updated trajectories $\{\tilde{\mathbf{u}}_i\}$, and then obtain $\{\tilde{\mathbf{x}}_i\}$. (3) We update the parameters θ of the energy-based model by maximum likelihood estimation, where the computation of the gradient of the likelihood is based on $\{\tilde{\mathbf{u}}_i\}$ and follows equation (4). (4) We update the parameters α of the trajectory generator by gradient descent on

$$\hat{L}'_g(\alpha) = \frac{\partial}{\partial \alpha} \left[\frac{1}{n} \sum_{i=1}^n \|\tilde{\mathbf{u}}_i - G_{\alpha}(\boldsymbol{\xi}_i, e_i, h_i)\|^2 \right]. \quad (11)$$

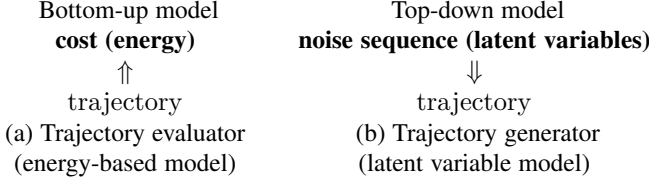
Algorithm 2 presents a detailed description of the cooperative training algorithm of an energy-based model and a trajectory generator for optimal control.

Algorithm 2 Energy-based IOC with a trajectory generator

- 1: **input** expert demonstrations $D = \{(\mathbf{x}_i, \mathbf{u}_i, e_i, h_i), \forall i\}$.
 - 2: **output** cost function parameters θ , and synthesized or optimized trajectories $\{(\tilde{\mathbf{x}}_i, \tilde{\mathbf{u}}_i), \forall i\}$.
 - 3: Let $\tau \leftarrow 0$, initialize θ .
 - 4: **repeat**
 - 5: **Initialization step:** Initialize $\hat{\mathbf{u}}_i = G_{\alpha_t}(\boldsymbol{\xi}_i, e_i, h_i)$, where $\boldsymbol{\xi}_i \sim p(\boldsymbol{\xi})$ by ancestral sampling, and then obtain $\tilde{\mathbf{x}}_i$ for each i .
 - 6: **Synthesis step or optimization step:** Given the initial $\hat{\mathbf{u}}_i$, synthesizing $\tilde{\mathbf{u}}_i \sim p_{\theta_t}(\mathbf{u}|e_i, h_i)$ by Langevin sampling, or optimizing $\tilde{\mathbf{u}}_i = \arg \min_{\mathbf{u}} C_{\theta}(\mathbf{x}, \mathbf{u}, e_i, h_i)$, by gradient descent (GD) or iLQR, and then obtain $\tilde{\mathbf{x}}_i$, for each i .
 - 7: **Analysis step (update cost function):** update $\theta_{\tau+1} = \theta_{\tau} + \gamma_{\tau} \hat{L}'(\theta_{\tau})$, where $\hat{L}'(\theta)$ is computed according to (4).
 - 8: **Analysis step (update policy model):** Update $\alpha_{\tau+1} = \alpha_{\tau} - \eta_{\tau} \hat{L}'_g(\alpha_{\tau})$, where \hat{L}'_g is computed according to (11).
 - 9: $\tau \leftarrow \tau + 1$.
 - 10: **until** $\tau = \tau_{\max}$, the number of iterations.
-

3.2 Bottom-up and top-down generative models of trajectories

Algorithm 2 presented in the main text is about a joint training of two types of generative models, the energy-based model (we also call it the trajectory evaluator) and the latent variable model (i.e., the trajectory generator). Both of these two models can be parameterized by deep neural networks and they are of opposite directions. The energy-based model has a bottom-up energy function that maps the trajectory to the cost, while the trajectory generator owns a top-down transformation that maps the sequence of noise vectors (i.e., the latent variables) to the trajectory, as illustrated by the following diagram.



3.3 Iterative and non-iterative generations of trajectories

The energy-based model $p_\theta(\mathbf{u}|e, h)$ defines a cost function or an energy function $C_\theta(\mathbf{x}, \mathbf{u}, e, h)$, from which we can derive the Langevin dynamics to generate \mathbf{u} . This is an implicit generation process of u that iterates the following Langevin step

$$\mathbf{u}_{s+1} = \mathbf{u}_s - \frac{\delta^2}{2} C'_\theta(\mathbf{x}_s, \mathbf{u}_s, e, h) + \delta \mathbf{z}_s, \quad (13)$$

where δ is the step size and s indexes the time step, $C'_\theta(\mathbf{x}, \mathbf{u}, e, h)$ is the derivative of the cost function with respect to \mathbf{u} . $\mathbf{z}_s \sim N(0, I)$ is the Brownian motion independently over time s , where I denotes the identity matrix of the same dimension as \mathbf{u} . Figure 1 (a) illustrates the generation process of (\mathbf{u}, \mathbf{x}) . Given (h, e) , the Langevin sampling seeks to find (u_1, \dots, u_T) to minimize the $C_\theta(\mathbf{x}, \mathbf{u}, e, h)$. The dashed double line arrows indicate iterative generation by sampling in the energy-based model, while the dashed line arrows indicate the known dynamic function $x_t = f(x_{t-1}, u_t)$. With the generated action sequence (u_1, \dots, u_T) , the state sequence (x_1, \dots, x_T) can be easily obtained by applying the dynamic function.

The trajectory generator generates (\mathbf{u}, \mathbf{x}) via ancestral sampling, $(\mathbf{u}, \mathbf{x}) = G_\alpha(\boldsymbol{\xi}, e, h)$ which is a non-iterative process to produce (\mathbf{u}, \mathbf{x}) from the recent history h (We assume $h = x_0$), environment e , and a sequence of noise vectors $\boldsymbol{\xi} = (\xi_1, \dots, \xi_T)$ serving as the latent variables. The generator can unfold over time and can be decomposed into the policy model $u_t = F_\alpha(x_{t-1}, \xi_t, e)$ and the dynamic function $x_t = f(x_{t-1}, u_t)$ at each time step. The latent variable ξ_t accounts for variation in the policy model at time step t . Figure 1(b) illustrates the generation process of the trajectory generator. The double line arrows indicate the mapping of the policy model, while the dashed line arrows indicate the known dynamic function. The whole process of generating (\mathbf{u}, \mathbf{x}) is of a dynamic or causal nature in that it directly evolves or unfolds over time.

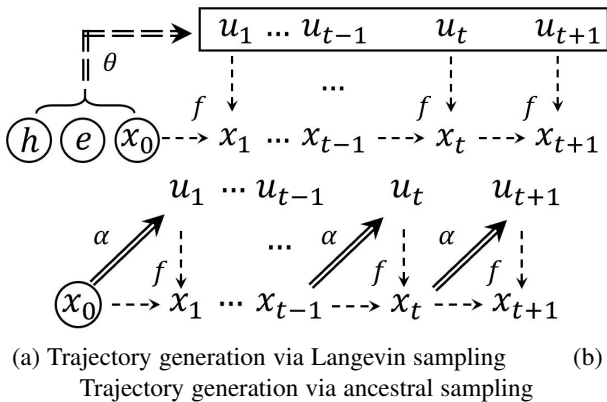


Fig. 1: Trajectory generation by (a) iterative method and (b) non-iterative method.

3.4 Issue in maximum likelihood training of the trajectory generator independently

Let $\boldsymbol{\xi} = (\xi_t, t = 1, \dots, T)$, where $\xi_t \sim N(0, I)$ independently over time t . Let $\mathbf{u} = (u_t, t = 1, \dots, T)$. We have $(12) \mathbf{u} = G_\alpha(\boldsymbol{\xi}, e, h) + \boldsymbol{\epsilon}$, where $\boldsymbol{\epsilon} = (\epsilon_t, t = 1, \dots, T)$ are observation errors and $\epsilon_t \sim N(0, \sigma^2 I)$. For notational simplicity, we omit \mathbf{x} and only keep \mathbf{u} in the output of G_α , because \mathbf{x} is just the intermediate output of G_α and \mathbf{u} is determined by \mathbf{x} . The trajectory generator defines the joint distribution of $(\mathbf{u}, \boldsymbol{\xi})$ conditioned on (e, h) as below,

$$q_\alpha(\mathbf{u}, \boldsymbol{\xi}|e, h) = q_\alpha(\mathbf{u}|\boldsymbol{\xi}, e, h)p(\boldsymbol{\xi}) \quad (14)$$

where $p(\boldsymbol{\xi}) = \prod_{i=1}^T p(\xi_i)$ is the prior distribution and $q_\alpha(\mathbf{u}|\boldsymbol{\xi}, e, h) = N(G_\alpha(\boldsymbol{\xi}, e, h), \sigma^2 I)$. The marginal distribution of \mathbf{u} conditioned on (e, h) is given by $q_\alpha(\mathbf{u}|e, h) = \int q_\alpha(\mathbf{u}, \boldsymbol{\xi}|e, h) d\boldsymbol{\xi}$. The posterior distribution is $q_\alpha(\boldsymbol{\xi}|\mathbf{u}, e, h) = q_\alpha(\mathbf{u}, \boldsymbol{\xi}|e, h)/q_\alpha(\mathbf{u}|e, h)$. Suppose we observe expert demonstrations $D = \{(\mathbf{u}_i, \mathbf{x}_i, e_i, h_i), i = 1, \dots, n\}$. The maximum likelihood estimation of α seeks to maximize the log-likelihood function given by

$$L(\alpha) = \sum_{i=1}^n \log q_\alpha(\mathbf{u}_i|e_i, h_i). \quad (15)$$

The learning gradient can be computed according to

$$\frac{\partial}{\partial \alpha} \log q_\alpha(\mathbf{u}|e, h) = \frac{1}{q_\alpha(\mathbf{u}|e, h)} \frac{\partial}{\partial \alpha} \int q_\alpha(\mathbf{u}, \boldsymbol{\xi}|e, h) d\boldsymbol{\xi} \quad (16)$$

$$= \int \left[\frac{\partial}{\partial \alpha} \log q_\alpha(\mathbf{u}, \boldsymbol{\xi}|e, h) \right] \frac{q_\alpha(\mathbf{u}, \boldsymbol{\xi}|e, h)}{q_\alpha(\mathbf{u}|e, h)} d\boldsymbol{\xi} \quad (17)$$

$$= \mathbb{E}_{q_\alpha(\boldsymbol{\xi}|\mathbf{u}, e, h)} \left[\frac{\partial}{\partial \alpha} \log q_\alpha(\mathbf{u}, \boldsymbol{\xi}|e, h) \right] \quad (18)$$

The expectation term in equation (18) is under the posterior distribution $q_\alpha(\boldsymbol{\xi}|\mathbf{u}, e, h)$ that is analytically intractable. One may draw samples from $q_\alpha(\boldsymbol{\xi}|\mathbf{u}, e, h)$ via Langevin inference dynamics that iterates

$$\boldsymbol{\xi}_{s+1} = \boldsymbol{\xi}_s + \frac{\delta^2}{2} \frac{\partial}{\partial \boldsymbol{\xi}} \log q_\alpha(\boldsymbol{\xi}_s|\mathbf{u}, e, h) + \delta \mathbf{z}_s, \quad (19)$$

where $\mathbf{z} \sim N(0, I)$, δ is the step size and s indexes the time step. Also, ξ_0 is usually sampled from Gaussian white noise for initialization. After we infer $\boldsymbol{\xi}$ from each observation (\mathbf{u}_i, e_i, h_i) by sampling from $q_\alpha(\boldsymbol{\xi}|\mathbf{u}_i, e_i, h_i)$ via Langevin inference process, the Monte Carlo approximation of the gradient of $L(\alpha)$ in equation (15) is computed by

$$\frac{\partial}{\partial \alpha} L(\alpha) \approx \frac{1}{n} \left[\frac{\partial}{\partial \alpha} \log q_\alpha(\mathbf{u}_i, \boldsymbol{\xi}_i|e_i, h_i) \right] \quad (20)$$

Since $\frac{\partial}{\partial \boldsymbol{\xi}} \log q_\alpha(\boldsymbol{\xi}|\mathbf{u}, e, h) = \frac{\partial}{\partial \boldsymbol{\xi}} \log q_\alpha(\mathbf{u}, \boldsymbol{\xi}|e, h)$ in equation (19). Both inference step in equation (19) and learning step in equation (20) need to compute derivative of $\log q_\alpha(\mathbf{u}, \boldsymbol{\xi}|e, h) = \frac{1}{2\sigma^2} \|G_\alpha(\boldsymbol{\xi}, e, h) - \mathbf{u}\|^2 + \text{const}$. The former is with respect to $\boldsymbol{\xi}$, while the latter is with respect to α , both of which can be computed by back-propagation through time. The resulting algorithm is called alternating back-propagation through time (ABPTT) algorithm [30].

Although the ABPTT algorithm is natural and simple, the difficulty of training the trajectory generator in this way might lie in the non-convergence issue of the short-run Langevin inference in equation (19). Even long-run Langevin inference chains are easy

to get trapped by local modes. Without fair samples drawn from the posterior distribution, the estimation of α will be biased.

3.5 Understanding the learning behavior of the cooperative training

In this section, we will present a theoretical understand of the learning behavior of the proposed Algorithm 2 shown in main text. We firstly start from the Contrastive Divergence (CD) algorithm that was proposed for efficient training of energy-based models. The CD runs k steps of MCMC initialized from the training examples, instead of the Gaussian white noise. Given the energy-based model for IOC $p_\theta(\mathbf{u}|e, h)$. Let M_θ be the transition kernel of the finite-step MCMC that samples from $p_\theta(\mathbf{u}|e, h)$. The original CD learning of $p_\theta(\mathbf{u}|e, h)$ seeks to minimize

$$\theta_{t+1} = \arg \min_{\theta} [\text{KL}(p_{\text{expert}}(\mathbf{u}|e, h) \| p_\theta(\mathbf{u}|e, h)) - \quad (21)$$

$$\text{KL}(M_{\theta_t} p_{\text{expert}}(\mathbf{u}|e, h) \| p_\theta(\mathbf{u}|e, h))], \quad (22)$$

where $p_{\text{expert}}(\mathbf{u}|e, h)$ is the unknown distribution of the observed demonstration of experts. Let $M_{\theta_t} p_{\text{expert}}(\mathbf{u}|e, h)$ denote the marginal distribution obtained after running S M_θ starting from $p_{\text{expert}}(\mathbf{u}|e, h)$. If $M_{\theta_t} p_{\text{expert}}(\mathbf{u}|e, h)$ converges to $p_\theta(\mathbf{u}|e, h)$, then the second KL-divergence will become very small, and the CD estimate eventually is close to maximum likelihood estimate which minimizes the first KL-divergence in equation (22).

In Algorithm 2, the MCMC sampling of the energy-based model is initialized from the trajectory generator $q_\alpha(\mathbf{u}|e, h)$, thus the learning of the energy-based model follows a modified CD estimate which, at time t , seeks to minimize

$$\theta_{t+1} = \arg \min_{\theta} [\text{KL}(p_{\text{expert}}(\mathbf{u}|e, h) \| p_\theta(\mathbf{u}|e, h)) - \quad (23)$$

$$\text{KL}(M_{\theta_t} q_\alpha(\mathbf{u}|e, h) \| p_\theta(\mathbf{u}|e, h))], \quad (24)$$

where we replace the $p_{\text{expert}}(\mathbf{u}|e, h)$ in equation (24) by $q_\alpha(\mathbf{u}|e, h)$. That means we run a finite-step MCMC from a given initial distribution $q_\alpha(\mathbf{u}|e, h)$, and use the resulting samples as synthesized examples to approximate the gradient of the log-likelihood of the EBM.

At time t , the learning of $q_\alpha(\mathbf{u}|e, h)$ seeks to minimize

$$\alpha_{t+1} = \arg \min_{\alpha} [\text{KL}(M_{\theta_t} q_{\alpha_t}(\mathbf{u}|e, h) \| q_\alpha(\mathbf{u}|e, h))]. \quad (25)$$

Equation (25) show that q_α learns to be the stationary distribution of M_θ . In other words, q_α seeks to be close to p_α , i.e., $q_\alpha \rightarrow p_\theta$. If so, the second KL-divergence term in equation (24) will become zero. The equation (24) is reduced to minimize the KL-divergence between the observed data distribution p_{expert} and the energy-based model p_θ . Eventually, q_α chases p_θ toward p_{expert} .

4 EXPERIMENTS

The code, more results and details can be found at : <http://www.stat.ucla.edu/~yifeixu/meioc>

4.1 Experimental setup

We evaluate the proposed energy-based inverse control methods on autonomous driving tasks.

In the task of autonomous driving, the state x_t consists of the coordinate, heading angle and velocity of the car, the control variables u_t consists of steering angle and acceleration, the environment e consists of road condition, speed limit, the curvature of the lane (which is represented by a cubic polynomial),

as well as the coordinates of other vehicles. The trajectories of other vehicles are treated as known environment states and assumed to remain unchanged while the ego vehicle is moving, even though the trajectories of other vehicles should be predicted in reality. In this paper, we sidestep this issue and focus on the inverse control problem.

We assume the dynamic function of all vehicle is a non-linear bicycle model [31]. It considers longitudinal, lateral and yaw motion under the assumption of negligible lateral weight shift, roll and compliance steer while travelling on a smooth road. Assume the current state of the vehicle is x_t, y_t, v_t, h_t (longitude, latitude, velocity, heading angle) and the action is a_t, θ_t (acceleration and steering angle). Then,

$$\begin{cases} r_t = & 3 + v_t \delta t \cos(\theta_t) - \sqrt{9 - (h_t \delta t \sin(\theta_t))^2}, \\ x_{t+1} = & x_t + \sin(\theta_t) r_t, \\ y_{t+1} = & y_t + \cos(\theta_t) r_t, \\ v_{t+1} = & x_t + a_t \delta t, \\ h_{t+1} = & x_t + \arcsin(\sin(\theta_t) v_t \delta t / \frac{3.043 v_t^2}{9.8}). \end{cases} \quad (26)$$

As to learning, the weight parameters are initialized by a normal distribution. The controls are also initialized by zeros, which is keeping straight. We normalize the controls, i.e., the steering and acceleration, because their scales are different. Instead of sampling the controls, we sample their changes. We set the number of steps of the Langevin dynamics or the gradient descent to be $l = 64$ and set the step size to be $\delta = 0.2$. The choice of l is a trade-off between computational efficiency and prediction accuracy. For parameter training, we use the Adam optimizer [32].

We use Root Mean Square Error (RMSE) in meters with respect to each timestep t to measure the accuracy of prediction, i.e., $RMSE(t) = \sqrt{\frac{1}{N} \sum_{i=1}^N \|\hat{y}_{it} - y_{it}\|^2}$, where N is the number of expert demonstrations, \hat{y}_{it} is the predicted coordinate of the i -th demonstration at time t and y_{it} is the ground truth coordinate of the i -th demonstration at time t . A small RMSE is desired. As a stochastic method, our method is also evaluated by average RMSE and minimum RMSE.

4.2 Dataset

We test our methods on two datasets. Massachusetts driving dataset focuses on highways with curved lanes and static scenes while NGSIM US-101 dataset focuses on rich vehicle interactions. We randomly split each dataset into training and testing sets.

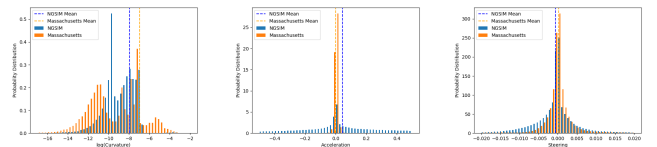


Fig. 2: Statistics comparison about Massachusetts Driving dataset and NGSIM dataset

(1) Massachusetts driving dataset: This is a private dataset collected from an autonomous vehicle during repeated trips on a stretch of highway. We shall make the dataset public once the paper is published. The dataset includes vehicle states and controls collected by the hardware on the vehicle and environment information. This dataset has a realistic driving scenario, which includes curved lanes and complex static scenes. To solve the

TABLE 1: List of hand-craft feature

Distance to the goal point in longitude	L2 norm of the accelerating value
Distance to the goal point in latitude	L2 norm of the steering value
Distance to the center of the lane	Difference to last accelerating value
Difference to the speed limit	Difference to last steering value
Difference to the direction of the lane	Distance to the nearest obstacle

TABLE 2: Generator Model

Layer	Output Size
concat($[x, e, \xi]$)	$6 + 29 + 4$
Linear, ReLU	64
Linear, ReLU	16
Linear, ReLU	8
Linear, Tanh	2

problem of noisy GPS signal, Kalman filtering is used to denoise the data. The number of trajectories is 44,000 with 0.1s intervals for a total of 4 seconds.

(2) NGSIM US-101: NGSIM [33] consists of real highway traffic captured at 10Hz over a time span of 45 minutes. Compared to Massachusetts driving dataset, NGSIM contains rich vehicle interactions. The control needs to consider other nearby vehicles. We preprocess the data by dividing the data into 5 seconds / 50 frames (10 for history and 40 to predict) blocks. There are 831 total scenes with 96,512 5-second vehicle trajectories. No control variables are provided. Thus, we need to infer the control of each vehicle given the vehicle state. Assuming bicycle model [31] dynamics, we perform an inverse-dynamics optimization using gradient descent to infer controls. The overall Root Mean Square Error (RMSE) compared to the ground truth GPS position is 0.97 meters. Since we use inferred trajectories, our preprocessed data are assumed to have perfect dynamics with noiseless and smooth control sequences and GPS coordinates.

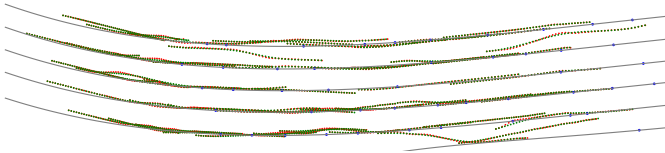


Fig. 3: Inferred trajectory compare to ground truth. (Green : Inferred; Red: Ground truth)

We provide a statistical comparison of two datasets. Figure 2 shows histograms for the road curvature, steering control, and acceleration control. We can see that Massachusetts has a bigger curvature while NGSIM has a much bigger acceleration. We think this is the biggest reason for the different results produced by gradient descent and iLQR.

Figure 3 shows a sample scene in inferred NGSIM dataset.

TABLE 3: CNN cost function network

Layer	Output Size	Stride
concat($[x, u, e]$)	$1 \times 40 \times (6 + 2 + 29)$	
hand-craft feature	$1 \times 40 \times 10$	
1×4 Conv1d, LeakyReLU	$1 \times 19 \times 32$	2
1×4 Conv1d, LeakyReLU	$1 \times 9 \times 64$	2
1×4 Conv1d, LeakyReLU	$1 \times 4 \times 128$	2
1×4 Conv1d, LeakyReLU	$1 \times 1 \times 256$	1
Linear	1	

TABLE 4: MLP cost function network

Layer	Output Size
concat($[x, u, e]$)	$6 + 2 + 29$
hand-craft feature	10
Linear, LeakyReLU	N_{hidden}
Linear, LeakyReLU	N_{hidden}
Linear	1

There are over 100 vehicles in this scene all move from left to right. Each dot sequence stands one vehicle from time frame 0 to frame 40. The green dot sequence represents the inferred trajectory and the red one represents ground truth.

4.3 Network Structure

We first use a linear combination of some hand-designed features as the cost function. Table 1 is the list of hand-craft feature defined in section 4.1. Feature normalization is adopted to make sure that each feature has the same scale of magnitude. It is used as a feature projector at the beginning of all cost function networks include our method via Langevin, GD, iLQR, and baseline methods. However, it is not used in the generator for joint training and GAIL.

Table 2 shows the generator model in joint training. It is similar to the actor network in GAIL’s PPO policy.

Table 4 and 3 are the MLP and CNN network structure we used in section 4.7. We further provide addition result by selecting different size of N_{hidden} and number of hidden layers in MLP setting in 4.10. It is set to 64 by default. Both table 2 and 4 are defined on a single frame while table 3 is defined on the whole trajectories. The number 40 in table 3 is the trajectory length.

4.4 Training Details

Normalization. We apply both pre-process normalization on controls and features. For the control value, we normalize each control value to have zero mean and variance of one according to the training set. We also normalize the different hand-designed features. We divided the feature by its means. For two datasets, we normalize them separately.

Optimizer. We use Adam optimizer on training all setting and network. All beta1 and beta2 are set to default 0.5. All initialize parameter is set as the Kaiming He initialization.

- Linear: Learning rate : 0.1; Exponential decay rate : 0.999
- MLP cost function: Learning rate : $5e-3$; No Exponential decay
- CNN cost function: Learning rate : $5e-3$; Exponential decay rate : 0.999
- Generator: Learning rate : $2e-3$; Exponential decay rate : 0.998

Langevin Dynamic. It happened sometime that the gradient will be too big. Also, the dynamic function will return NaN if a too big control value is fed. As a result, we set the maximum limit for each step in Langevin dynamic / gradient descent to 0.1 for both action. The step size is set as 0.1 and the number of steps set as 64. All settings are the same for gradient descent. In appendix 3, we do an ablation study on the different settings of step number and step size.

iLQR In iLQR solver, we grid search the learning rate from 0.001 to 1. The maximum step is set as 100. If the difference to the previous step is smaller than 0.001, the early-stop is triggered. In the experiment, the average iLQR step is around 30.

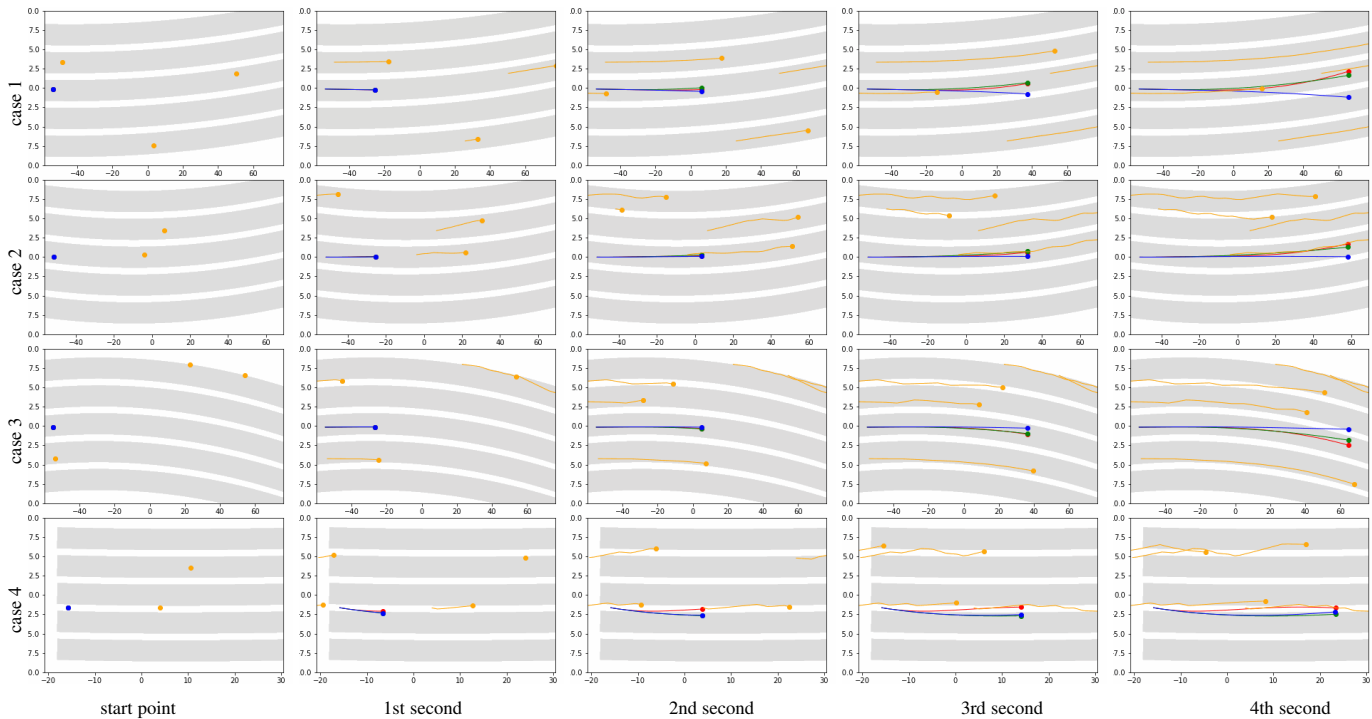


Fig. 4: Predicted trajectories for single-agent control. (Green: Predicted trajectories (Ours). Blue: Predicted trajectories (GAIL). Red: Ground truths. Orange: Other vehicles. Gray: Lanes.)

Training time. We use a mini-batch of size 1024 during training. For the joint learning setting, we update the generator 5 times for each synthesis step. For each epoch, we shuffle the whole dataset. That is, every iteration has a different mini-batch. The following is the time consumption for each epoch while training on Massachusetts driving dataset. The train time is counted on i9-9900 + Tesla P100.

- Linear: It takes around 3 minutes for each epoch, 40 epochs in total. Training time is dominated by the number of steps we choose. If we decrease the step number to 8, it takes 40 seconds per epoch.
- MLP / CNN cost function: It takes around 10 minutes for each epoch, 40 epochs in total.
- Joint training: Learning rate: It takes around 3 minutes for each epoch, 40 epochs in total.
- GAIL: GAIL uses a smaller mini-batch size of 64. It takes around 10 minutes for each epoch. 40 epochs in total.
- CIOC: It takes around 1 minute for each epoch, 40 epochs in total.

4.5 Single-agent control

We first test our methods, including sampling-based and optimization-based ones, on single-agent control problem. We compare our method with three baseline methods.

- Constant velocity: the simplest baseline with a constant velocity and zero steerings.
- Generative adversarial imitation learning (GAIL) [17]: The original GAIL method was proposed for imitation learning. We use the same setting as in [34], which applies GAIL to the task of modeling human highway driving behavior. Besides, we change the policy gradient method from Trust Region Policy Optimization (TRPO) [35] to Proximal Policy Optimization (PPO) [36].

- CIOC with Laplace [20]: We implement this baseline with the same iLQR method as that in our model.

We can predict the full trajectories with 64 steps of Langevin dynamics (or gradient descent) in roughly 0.1 second. Figure 4 displays some example results. Each point sequence represents a 3-second trajectory over time from left to right. Table 5 and 6 show the results for Massachusetts driving dataset and NGSIM, respectively. In the last two rows, we provide both average RMSE along with the minimum RMSE for our sampling-based approach. Our methods achieve substantial improvements compared to baseline methods, such as CIOC [20] and GAIL, in terms of testing RMSE. We find that the sampling-based methods outperform the optimization-based methods among our energy-based approaches.

TABLE 5: Massachusetts driving dataset result.

Method	1s	2s	3s
Constant Velocity	0.340	0.544	1.023
CIOC with Laplace	0.386	0.617	0.987
GAIL	0.368	0.626	0.977
ours (via iLQR)	0.307	0.491	0.786
ours (via GD)	0.257	0.413	0.660
ours AVG (via Langevin)	0.255	0.401	0.637
ours MIN (via Langevin)	<i>0.157</i>	<i>0.354</i>	<i>0.607</i>

The reason why the method “CIOC with Laplace” performs poorly on both two datasets is due to the fact that its Laplace approximation is not accurate enough for a complex cost function used in the current tasks. Our models are more genetic and do not make such an approximation. Instead, they use Langevin sampling for maximum likelihood training. Therefore, our methods can provide more accurate prediction results.

The problem of GAIL is due to its model complexity. GAIL parameterizes its discriminator, policy and value function by MLPs.

TABLE 6: NGSIM dataset result.

Method	1s	2s	3s	4s
Constant Velocity	0.569	1.623	3.075	4.919
CIOC with Laplace	0.503	1.468	2.801	4.530
GAIL	0.367	0.738	1.275	2.360
ours (via iLQR)	0.351	0.603	0.969	1.874
ours (via GD)	0.318	0.644	1.149	2.138
ours AVG (via Langevin)	0.311	0.575	0.880	1.860
ours MIN (via Langevin)	<i>0.203</i>	<i>0.458</i>	<i>0.801</i>	<i>1.690</i>

Designing optimal MLP structures of these components for GAIL is challenging. Our method only needs to design a single architecture for the cost function. Additionally, our method for optimal control is performed by simulating the trajectory of actions and states according to the learned cost function taking into account the future information. In contrast, GAIL relies on its learned policy net for step-wise decision making.

Compared with gradient descent (optimization-based approach), Langevin dynamics-based method can obtain smaller errors. One reason is that the sampling-based approach rigorously maximizes the log-likelihood of the expert demonstrations during training, while the optimization-based approach is just a convenient approximation. The other reason is that the Gaussian noise term in each Langevin step helps to explore the cost function and avoid sub-optimal solutions.

4.6 Corner case testing with toy examples

Corner cases are important for model evaluation. We construct 6 typical corner cases to test our model. Figure 5 shows the predicted trajectories by our method for several cases. Figures 5(a) and (b) show two cases of sudden braking. In each of the cases, a vehicle (orange) in front of the ego vehicle (green) is making a sudden brake. In case (a), there are not any other vehicles moving alongside the ego vehicle, so it is predicted to firstly change the lane, then accelerate past the vehicle in front, and return to its previous lane and continue its driving. In case (b), two vehicles are moving alongside the ego vehicle. The predicted trajectory shows that the ego vehicle is going to trigger a brake to avoid a potential collision accident. Figures 5(c) and (d) show two cases in cut-in situation. In each case, a vehicle is trying to cut in from the left or right lane. The ego vehicle is predicted to slow down to ensure the safe cut-in of the other vehicle. Figures 5(e) and (f) show two cases in the large lane curvature situation, where our model can still perform well to predict reasonable trajectories.

Figure 6 shows the corresponding plots of the predicted controls over time steps. In each plot, blue lines stand for acceleration and orange lines stand for steering. The dash lines represent the initialization of the control for Langevin sampling, which is actually the control at the last time step in the history trajectory. We use 64 Langevin steps to sample the controls from the learned cost function. We plot the predicted control (i.e., acceleration and steering) over time for each Langevin step. The curves with more numbers of Langevin steps appear darker. Thus, the darkest solid lines are the final predicted control.

In short, this experiment demonstrates that our method is capable of learning a reasonable cost function to handle corner cases, such as situations of sudden braking, lane cut-in, and making turns in curved lanes.

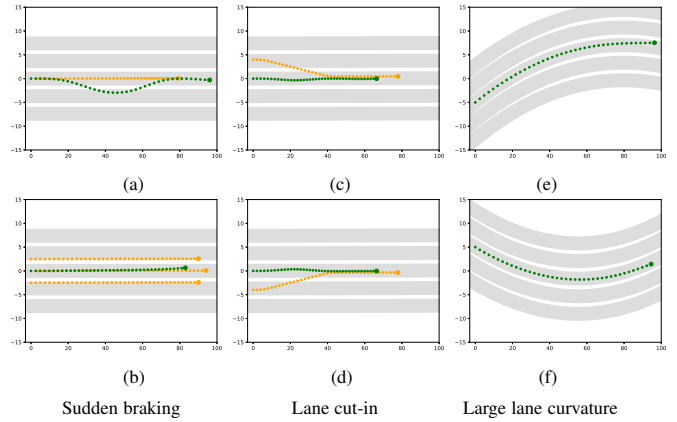


Fig. 5: Predicted trajectories in corner cases. (Green : predicted trajectories. Orange : trajectories of other vehicles. Gray: Lanes.)

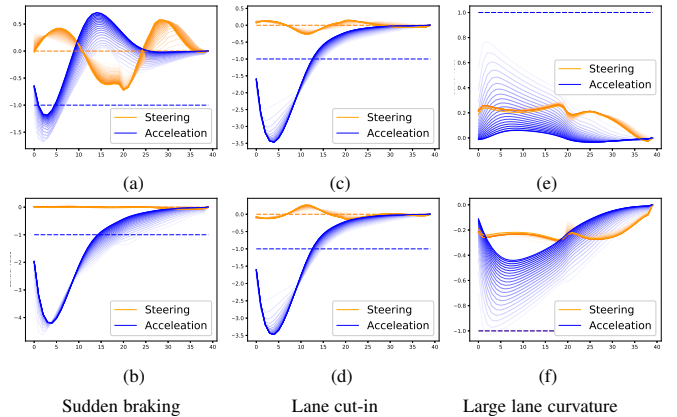


Fig. 6: Predicted control over time. (dash lines: initial values of the controls for Langevin sampling. solid lines: predicted controls over time steps. Blue: control of acceleration. Orange: control of steering.)

4.7 Evaluation of different cost functions

The Neural network is a powerful function approximator. It is capable of approximating any complex nonlinear function given sufficient training data, and it is also flexible to incorporate prior information, which in our case are the manually designed features. In this experiment, we replace the linear cost function in our sampling-based approach with a neural network. Specifically, we design a cost function by multilayer perceptron (MLP), where we put three layers on top of the vector of hand-designed features: $C_\theta(\mathbf{x}, \mathbf{u}, e, h) = f(\phi(\mathbf{x}, \mathbf{u}, e, h))$, where f contains 2 hidden layers and 1 output layer. We also consider using a 1D CNN that takes into account the temporal relationship inside the trajectory for the cost function. We add four 1D convolutional layers on top of the vector of hand-designed features, where the kernel size in each layer is 1×4 . The numbers of channels are $\{32, 64, 128, 256\}$ and the numbers of strides are $\{2, 2, 2, 1\}$ for different layers, respectively. One fully connected layer with a single kernel is attached at the end.

Table 7 shows the performance of different designs of cost functions. We can see that improvements can be obtained by using cost functions parameterized by either MLP or CNN. Neural network provides nonlinear connection layers as a transformation of the original input features. This implies that there are some internal

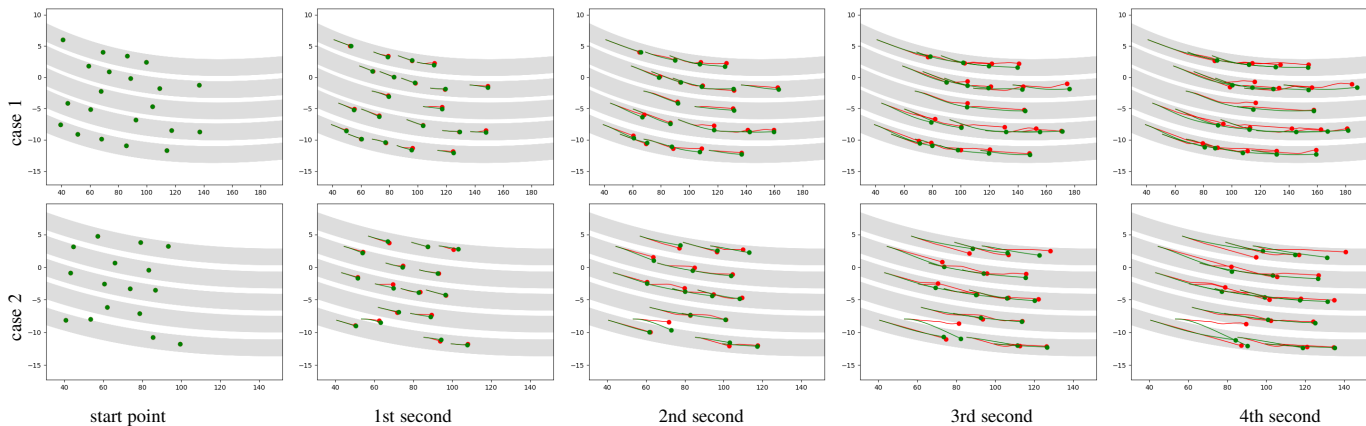


Fig. 7: Predicted trajectories for multi-agent control. (Green: Predicted trajectories. Red: Ground truths. Gray: Lanes.)

connections between the features and some temporal connections among feature vectors at different time steps.

TABLE 7: Performance of models with different cost functions.

Method (RMSE)	1s	2s	3s
Linear	0.255	0.401	0.637
MLP	0.237	0.379	0.607
CNN	0.234	0.372	0.572

4.8 Multi-agent control

In the setting of single-agent control, the future trajectories of other vehicles are assumed to be known (e.g., they are predicted by a prediction method) and they remain unchanged no matter how the ego vehicle moves. We extend our framework to multi-agent setting. In this setting, we simultaneously control all vehicles in the scene. The controls of other vehicles are used to predict the trajectories of other vehicles.

Suppose there are K agents, and every agent in the scene can be regarded as a general agent. The state and control space are Cartesian products of the individual states and controls respectively, i.e., $\mathbf{X} = (\mathbf{x}^k, k = 1, 2, \dots, K)$, $\mathbf{U} = (\mathbf{u}^k, k = 1, 2, \dots, K)$. All the agents share the same dynamic function, which is $x_t^k = f(x_{t-1}^k, u_t^k) \forall k = 1, 2, \dots, K$. The overall cost function are set to be the sum of each agent $C_\theta(\mathbf{X}, \mathbf{U}, e, h) = \sum_{k=0}^K C_\theta(\mathbf{x}^k, \mathbf{u}^k, e, h^k)$. Thus, the conditional probability density function becomes $p_\theta(\mathbf{U}|e, h) = \frac{1}{Z_\theta(e, h)} \exp[-C_\theta(\mathbf{X}, \mathbf{U}, e, h)]$, where $Z_\theta(e, h)$ is the intractable normalizing constant.

We compare our method with the following baselines for multi-agent control.

- Constant velocity: The simplest baseline with a constant velocity and zero steerings.
- The parameter sharing GAIL (PS-GAIL) [37] [38]: This method extends single-agent GAIL and Parameter Sharing Trust Region Policy Optimization (PS-TRPO) [39] to enable imitation learning in the multi-agent context.

We test our method on the NGSIM dataset. We use a linear cost function setting for each agent in this experiment. The maximum number of agents is 64. Figure 7 shows three examples of the qualitative results, one per column. The first to fourth rows show the positions of all vehicles in the scene as dots after 1 to 4 seconds respectively, along with the predicted trajectories (the green lines)

and the ground truths (the red lines). Table 8 shows a comparison of performance between our method and the baselines. Results show that our method can work well in the multi-agent control scenario.

TABLE 8: Performance comparison in multi-agent control on NGSIM dataset. RMSEs are reported.

Method	1s	2s	3s	4s
Constant Velocity	0.569	1.623	3.075	4.919
PS-GAIL	0.602	1.874	3.144	4.962
ours (multi-agent)	0.365	0.644	1.229	2.262

4.9 Joint training with trajectory generator

In this section, we follow algorithm 2 to introduce a trajectory generator as a fast initializer for our Langevin sampler. In the experiment, we design F_α as a 3-layer MLP with hidden dimensions 64, 16 and 8, respectively, at different layers. The activation function is ReLU for each hidden layer and Tanh for the final layer. The learning rate of the trajectory generator is set to be 0.005. The rest of the setting remains the same as in the model with a linear cost function.

TABLE 9: Joint training with trajectory generator (average RMSE)

Number of steps	2	8	16	32	64
w/o generator	0.845	0.746	0.709	0.672	0.636
fast initializer	0.956	0.835	0.844	0.845	0.854
with generator	0.804	0.672	0.649	0.638	0.633
generator only	0.911				

Table 9 compares the proposed joint training method with the following baselines in terms of average RMSE. The methods include (1) “w/o generator”: the single EBM method without using a trajectory generator. (2) “fast initializer”: the trajectory generator trained with an EBM via the proposed cooperative training algorithm. We train both methods (1) and (2) as well as our method (which we refer to as “with generator” in Table (9) with different numbers of Langevin steps. Besides, we implement method (3), which is a single trajectory generator trained via maximum likelihood estimation.

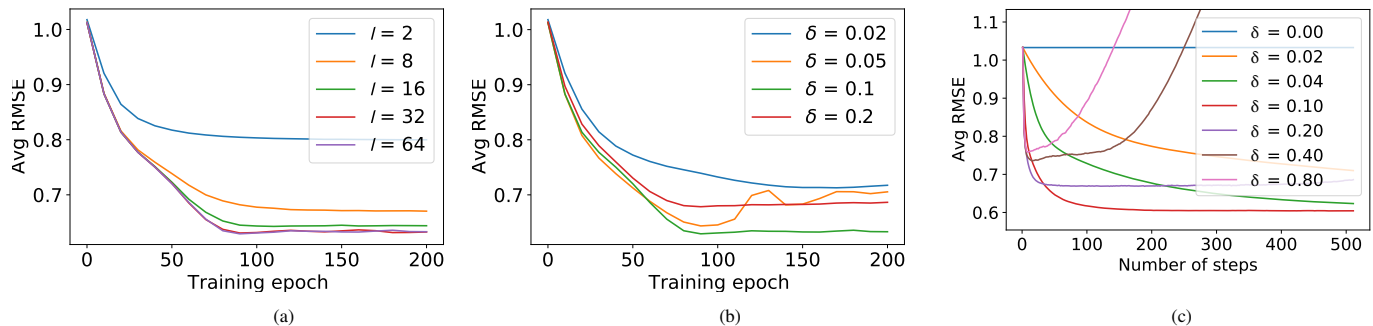


Fig. 8: Influence of hyperparameters. (a) a line chart of testing average RMSEs over training epochs for different numbers of Langevin steps used in training. (b) a line chart of testing average RMSEs over training epochs for different Langevin step sizes used in training. (c) Influence of different numbers of Langevin steps and step sizes used in training. (d) Influence of different numbers of Langevin steps and step sizes used in testing.

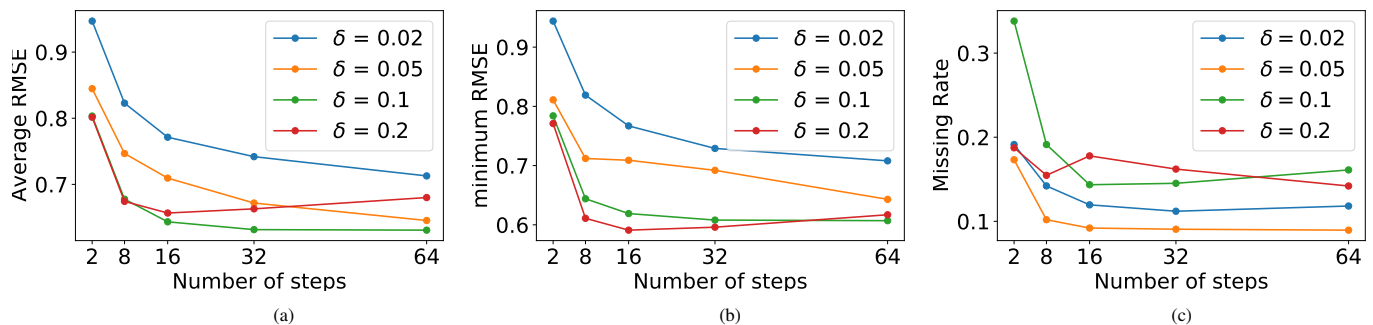


Fig. 9: Performance comparison of energy-based models with different numbers of Langevin steps and Langevin step sizes. Each curve represents a model with a certain Langevin step size δ . We set $\delta=0.02, 0.05, 0.1$ and 0.2 . For each setting of δ , we choose different numbers of steps $l=2, 8, 16, 32$ and 64 . Performances are measured by (a) Average RMSE (b) minimum RMSE (c) missing rate on Massachusetts driving dataset.

This comparison results show that a fast initializer can improve the performance even with less Langevin steps. For example, a model using 8 Langevin steps with a fast initializer is comparable with the one with a 32-step Langevin dynamics. Also, the method of “fast initializer” performs better than the “generator only” setting because of the guidance of Langevin sampling of the EBM.

4.10 Ablation Study for energy-based IOC models

4.10.1 Influence of hyperparameters

We investigate the influence of different choices of some hyperparameters in training, such as the number of Langevin steps l and the Langevin step size δ .

We firstly study the influence of different choices of some hyperparameters, such as the number of Langevin steps l , and the step size δ of each Langevin. Figure 9 depicts the performances of energy-based IOC models with different δ and l on Massachusetts driving dataset. Each curve is associated with a certain step size δ and shows the testing performances over different numbers of Langevin steps. The performances are measured by average RMSE, minimum RMSE and missing rate. Missing rate is defined as the number of trajectories where none of the predicted trajectories are within 1.0 meters of ground truth according to endpoint error. The three metrics are used in the sub-figures of Figure 9, respectively. In general, with the same δ , the model performance increases as the number of Langevin steps increases. However, the performance gains become smaller and smaller while using more Langevin steps.

Using more Langevin steps will also increase the computational time of sampling. We use $l = 64$ to make a trade-off between performance and computational efficiency. We also choose $\delta = 0.1$ for a trade-off among performances measured by different metrics.

Figures 8(a) and (b) depict training curves of the models with different l and δ , respectively. The models are trained on the Massachusetts driving dataset. Each curve reports the testing average RMSEs over training epochs. For testing, we use the same l and δ as those in training. We observe that the learning is quite stable in the sense that the testing errors drop smoothly with an increasing number of training epochs.

We also study, given a trained model, how different choices of l and δ in testing can affect the performance of the model. Figure 8(c) shows the average RMSEs of trajectories that are sampled from a learned model by using different numbers of Langevin steps l and step sizes δ . The model we use is with a linear cost function and trained with $l = 64$ and $\delta = 0.1$. We observe that: in the testing stage, using Langevin step sizes smaller than that in the training stage may take more Langevin steps to converge, while using larger ones may lead to a non-convergence issue. Thus, we suggest using the same l and δ in both training and testing stages for optimal performance.

4.10.2 Joint training of an energy-based model with a trajectory generator

We hence study the influence of different choices of the number of Langevin steps l and the Langevin step size δ in the coop-

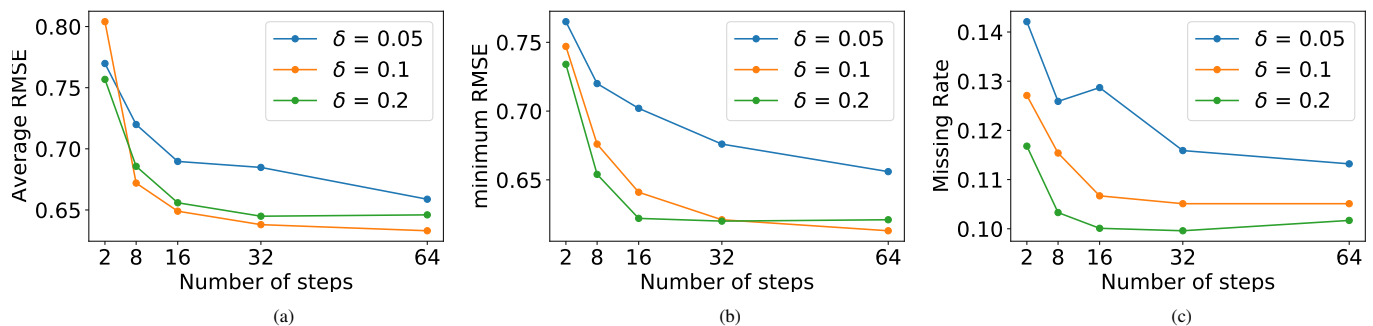


Fig. 10: Model analysis for the cooperative training frameworks. Performance comparison of frameworks using different numbers of Langevin steps and different Langevin step sizes. Each curve represents a framework with a certain Langevin step size δ . We set $\delta=0.05, 0.1$ and 0.2 . For each setting of δ , different numbers of Langevin steps are chosen, $l=2, 8, 16, 32$ and 64 . Performances are measured by three different metrics, which are (a) Average RMSE (b) minimum RMSE, and (c) missing rate.

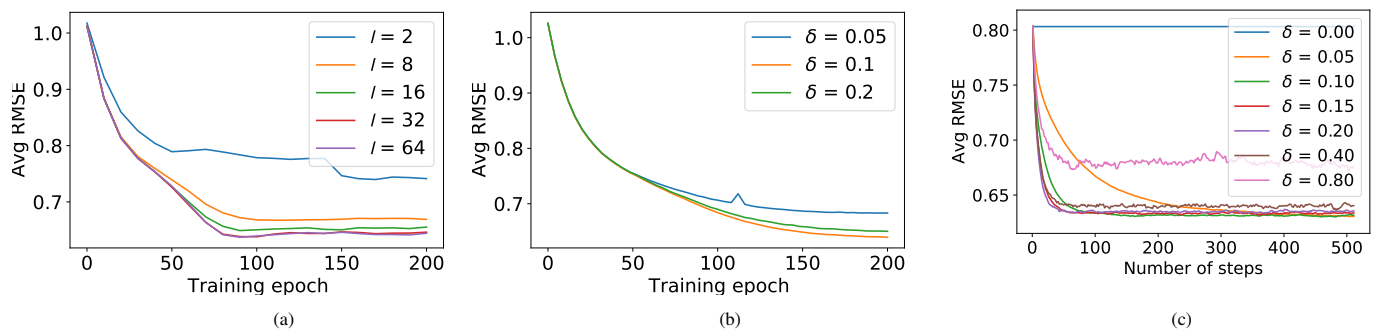


Fig. 11: (a) Testing performances during the cooperative training with different Langevin steps l . (b) Testing performances during the cooperative training with different Langevin step size δ . (c) Testing performance after training. Each curve shows testing performances over different numbers of Langevin steps used to sample trajectories in testing. Each curve is associated with a step size chosen in testing. The model is trained with the Langevin step size $\delta = 0.2$ and the number of steps $l = 32$.

erative training framework. Figure 10 depicts the performances of cooperative training frameworks with different δ and l on Massachusetts driving dataset. The performances shown in Figures 10(a) 10(b) and 10(c) are measured by average RMSE, minimum RMSE and missing rate, respectively. Each curve corresponds to a framework with a certain step size δ and shows the testing performances over different numbers of Langevin steps. Fixing δ , the model performance increases as the number of Langevin steps increases. We use $l = 32$ and $\delta = 0.1$ to make a trade-off between performance and computational efficiency.

Figure 11 (a) and (b) shows the learning curves of the cooperative training with different numbers of Langevin steps and different step sizes, respectively. Each learning curve shows testing average RMSE over different of training epochs. We observe that the testing average RMSE decreases smoothly as the number of training epochs increases. We also study how different l and δ chosen in testing affect the performance of a learned energy-based IOC model. We first train an energy-based model with $\delta = 0.2$ and $l = 32$, and use the learned model in testing with varying Langevin step size δ and number of Langevin steps l . Figure 11 (c) depicts the influences of varying δ and l in testing. We observe that given a learned cost function, Langevin sampling with smaller step size and a larger number of Langevin steps may allow the model to generate better trajectories.

Figure 12 (a) and (b) shows the testing performances over different training epochs for the trajectory generators trained in the

cooperative training framework with different numbers of Langevin steps and different step sizes, respectively.

Figure 13 provides a performance comparison and training curves for models using different types of MLP cost functions. We observe that 4 layer MLP with 32 hidden dimension performs the best.

5 CONCLUSION

This paper studies the fundamental problem of learning the cost function from expert demonstrations for continuous optimal control. We study this problem in the framework of the energy-based model, and we propose a sampling-based method and optimization-based modification to learn the cost function. Unlike the previous method for continuous inverse control [20], we learn the model by maximum likelihood using Langevin sampling, without resorting to Laplace approximation. This is a possible reason for improvement over the previous method. Langevin sampling or MCMC sampling in general also has the potential to avoid sub-optimal modes. Moreover, we propose to train the energy-based model with a trajectory generator as a fast initializer to improve the learning efficiency. The experiments show that our method is generally applicable, and can learn non-linear and non-Markovian cost functions.

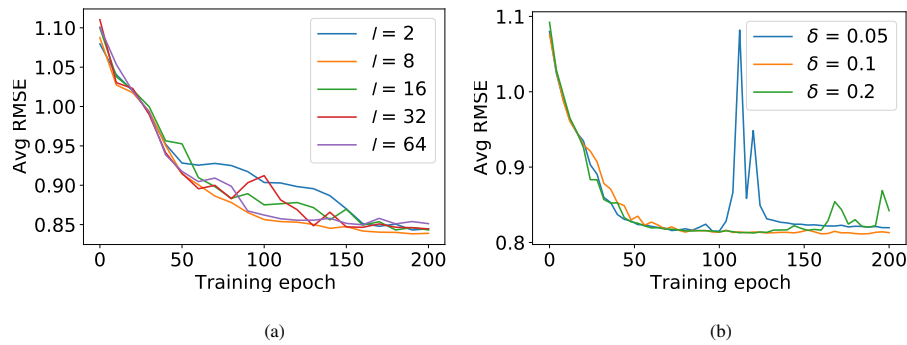


Fig. 12: (a) Testing performances over different training epochs of the trajectory generators trained in the cooperative training framework with different numbers of Langevin steps l . (b) Testing performances over different training epochs of the trajectory generators trained in the cooperative training framework with different Langevin step size δ .

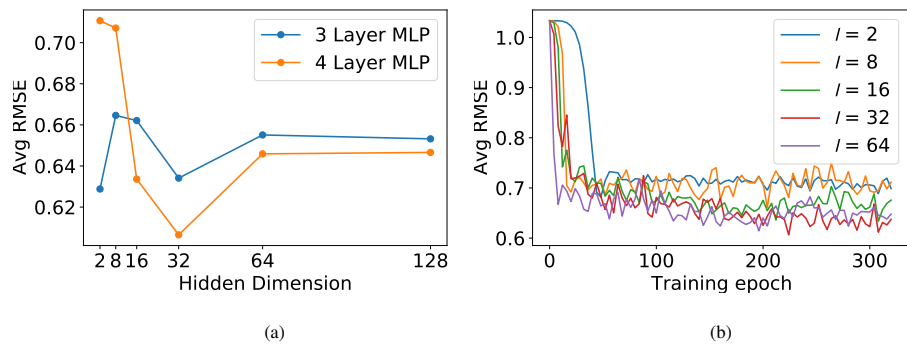


Fig. 13: (a) Model analysis for different setting of MLP cost functions comparison. Average RMSE result for different MLP structures (b) Testing performances over different training epochs with different hidden dimensions for 4 layer MLP.

ACKNOWLEDGMENTS

The work is supported by NSF DMS-2015577, DARPA SIMPLEX N66001-15-C-4035, ONR MURI N00014-16-1-2007, DARPA ARO W911NF-16-1-0579, DARPA N66001-17-2-4029, and XSEDE grant ASC180018.

REFERENCES

- [1] E. Todorov, “Optimal control theory,” *Bayesian brain: probabilistic approaches to neural coding*, pp. 269–298, 2006.
- [2] W. Li and E. Todorov, “Iterative linear quadratic regulator design for nonlinear biological movement systems,” in *ICINCO (1)*, 2004, pp. 222–229.
- [3] A. Bemporad, M. Morari, V. Dua, and E. N. Pistikopoulos, “The explicit linear quadratic regulator for constrained systems,” *Automatica*, vol. 38, no. 1, pp. 3–20, 2002.
- [4] R. M. Neal *et al.*, “Mcmc using hamiltonian dynamics,” *Handbook of markov chain monte carlo*, vol. 2, no. 11, p. 2, 2011.
- [5] B. D. Ziebart, A. L. Maas, J. A. Bagnell, and A. K. Dey, “Maximum entropy inverse reinforcement learning,” in *AAAI*, vol. 8. Chicago, IL, USA, 2008, pp. 1433–1438.
- [6] S. C. Zhu, Y. Wu, and D. Mumford, “Filters, random fields and maximum entropy (frame): Towards a unified theory for texture modeling,” *International Journal of Computer Vision*, vol. 27, no. 2, pp. 107–126, 1998.
- [7] M. Richardson and P. Domingos, “Markov logic networks,” *Machine learning*, vol. 62, no. 1-2, pp. 107–136, 2006.
- [8] M. Wulfmeier, P. Ondruska, and I. Posner, “Maximum entropy deep inverse reinforcement learning,” *arXiv preprint arXiv:1507.04888*, 2015.
- [9] J. Xie, S.-C. Zhu, and Y. N. Wu, “Learning energy-based spatial-temporal generative convnets for dynamic patterns,” *IEEE transactions on pattern analysis and machine intelligence*, 2019.
- [10] J. Xie, W. Hu, S.-C. Zhu, and Y. N. Wu, “Learning sparse frame models for natural image patterns,” *International Journal of Computer Vision*, vol. 114, no. 2-3, pp. 91–112, 2015.
- [11] J. Xie, S.-C. Zhu, and Y. N. Wu, “Synthesizing dynamic patterns by spatial-temporal generative convnet,” in *Proceedings of the IEEE Conference on Computer Vision and Pattern Recognition*, 2017, pp. 7093–7101.
- [12] Y. LeCun, Y. Bengio *et al.*, “Convolutional networks for images, speech, and time series,” *The handbook of brain theory and neural networks*, vol. 3361, no. 10, p. 1995, 1995.
- [13] A. Krizhevsky, I. Sutskever, and G. E. Hinton, “Imagenet classification with deep convolutional neural networks,” in *Advances in neural information processing systems*, 2012, pp. 1097–1105.
- [14] C. Finn, S. Levine, and P. Abbeel, “Guided cost learning: Deep inverse optimal control via policy optimization,” in *International Conference on Machine Learning*, 2016, pp. 49–58.
- [15] C. Finn, P. Christiano, P. Abbeel, and S. Levine, “A connection between generative adversarial networks, inverse reinforcement learning, and energy-based models,” *arXiv preprint arXiv:1611.03852*, 2016.
- [16] I. Goodfellow, J. Pouget-Abadie, M. Mirza, B. Xu, D. Warde-Farley, S. Ozair, A. Courville, and Y. Bengio, “Generative adversarial nets,” in *Advances in neural information processing systems*, 2014, pp. 2672–2680.
- [17] J. Ho and S. Ermon, “Generative adversarial imitation learning,” in *Advances in Neural Information Processing Systems*, 2016, pp. 4565–4573.
- [18] Y. Li, J. Song, and S. Ermon, “Infogail: Interpretable imitation learning from visual demonstrations,” in *Advances in Neural Information Processing Systems*, 2017, pp. 3812–3822.
- [19] M. Monfort, A. Liu, and B. D. Ziebart, “Intent prediction and trajectory forecasting via predictive inverse linear-quadratic regulation,” in *Proceedings of the Twenty-Ninth AAAI Conference on Artificial Intelligence*, ser. AAAI’15. AAAI Press, 2015, pp. 3672–3678. [Online]. Available: <http://dl.acm.org/citation.cfm?id=2888116.2888226>
- [20] S. Levine and V. Koltun, “Continuous inverse optimal control with locally optimal examples,” *arXiv preprint arXiv:1206.4617*, 2012.
- [21] A. Alahi, K. Goel, V. Ramanathan, A. Robicquet, L. Fei-Fei, and S. Savarese, “Social lstm: Human trajectory prediction in crowded spaces,”

- in *Proceedings of the IEEE International Conference on Computer Vision and Pattern Recognition*, 2016.
- [22] A. Gupta, J. Johnson, L. Fei-Fei, S. Savarese, and A. Alahi, “Social gan: Socially acceptable trajectories with generative adversarial networks,” in *Proceedings of the IEEE International Conference on Computer Vision and Pattern Recognition*, 2018.
- [23] A. Vemula, K. Muelling, and J. Oh, “Social attention: Modeling attention in human crowds,” in *Proceedings of the International Conference on Robotics and Automation (ICRA) 2018*, May 2018.
- [24] N. Lee, W. Choi, P. Vernaza, C. B. Choy, P. H. Torr, and M. Chandraker, “Desire: Distant future prediction in dynamic scenes with interacting agents,” in *Proceedings of the IEEE Conference on Computer Vision and Pattern Recognition*, 2017, pp. 336–345.
- [25] N. Deo, A. Rangesh, and M. M. Trivedi, “How would surround vehicles move? a unified framework for maneuver classification and motion prediction,” *IEEE Transactions on Intelligent Vehicles*, vol. 3, no. 2, pp. 129–140, 2018.
- [26] T. Zhao, Y. Xu, M. Monfort, W. Choi, C. Baker, Y. Zhao, Y. Wang, and Y. N. Wu, “Multi-agent tensor fusion for contextual trajectory prediction,” in *The IEEE Conference on Computer Vision and Pattern Recognition (CVPR)*, June 2019.
- [27] H. Robbins and S. Monro, “A stochastic approximation method,” *The annals of mathematical statistics*, pp. 400–407, 1951.
- [28] J. Xie, Y. Lu, R. Gao, S.-C. Zhu, and Y. N. Wu, “Cooperative training of descriptor and generator networks,” *IEEE transactions on pattern analysis and machine intelligence*, vol. 42, no. 1, pp. 27–45, 2018.
- [29] J. Xie, Z. Zheng, X. Fang, S.-C. Zhu, and Y. N. Wu, “Cooperative training of fast thinking initializer and slow thinking solver for multi-modal conditional learning,” *arXiv preprint arXiv:1902.02812*, 2019.
- [30] J. Xie, R. Gao, Z. Zheng, S.-C. Zhu, and Y. N. Wu, “Learning dynamic generator model by alternating back-propagation through time,” in *Proceedings of the AAAI Conference on Artificial Intelligence*, vol. 33, 2019, pp. 5498–5507.
- [31] P. Polack, F. Altché, B. d’Andréa Novel, and A. de La Fortelle, “The kinematic bicycle model: A consistent model for planning feasible trajectories for autonomous vehicles?” in *Intelligent Vehicles Symposium (IV), 2017 IEEE*. IEEE, 2017, pp. 812–818.
- [32] D. P. Kingma and J. Ba, “Adam: A method for stochastic optimization,” *arXiv preprint arXiv:1412.6980*, 2014.
- [33] J. Colyar and J. Halkias, “Us highway dataset,” vol. Federal Highway Administration (FHWA), Tech. Rep. FHWA-HRT-07-030, 2007.
- [34] A. Kuefler, J. Morton, T. Wheeler, and M. Kochenderfer, “Imitating driver behavior with generative adversarial networks,” in *Intelligent Vehicles Symposium (IV), 2017 IEEE*. IEEE, 2017, pp. 204–211.
- [35] J. Schulman, S. Levine, P. Abbeel, M. Jordan, and P. Moritz, “Trust region policy optimization,” in *International conference on machine learning*, 2015, pp. 1889–1897.
- [36] J. Schulman, F. Wolski, P. Dhariwal, A. Radford, and O. Klimov, “Proximal policy optimization algorithms,” *arXiv preprint arXiv:1707.06347*, 2017.
- [37] R. P. Bhattacharyya, D. J. Phillips, B. Wulfe, J. Morton, A. Kuefler, and M. J. Kochenderfer, “Multi-agent imitation learning for driving simulation,” in *2018 IEEE/RSJ International Conference on Intelligent Robots and Systems (IROS)*. IEEE, 2018, pp. 1534–1539.
- [38] R. P. Bhattacharyya, D. J. Phillips, C. Liu, J. K. Gupta, K. Driggs-Campbell, and M. J. Kochenderfer, “Simulating emergent properties of human driving behavior using multi-agent reward augmented imitation learning,” in *Proceedings of the International Conference on Robotics and Automation (ICRA)*, May 2019.
- [39] J. K. Gupta, M. Egorov, and M. Kochenderfer, “Cooperative multi-agent control using deep reinforcement learning,” in *International Conference on Autonomous Agents and Multiagent Systems*. Springer, 2017, pp. 66–83.